

New derivation of redshift distance without using power expansions. II. Additional redshift distances, analyzing the data of more quasars, of some SNIa, of the one black hole in galaxy M87 as well as a newer estimation of H_0

Steffen Haase*¹

*04319 Leipzig, Germany

Abstract

In this part of the two-part series of essays, we first derive some equations for further physical redshift distances. We then analyze a catalog with 132,975 quasars, for which both the apparent magnitude m and the redshift z are given, in order to find the today's value of the parameter β_0 of the theory presented. We then use this value to determine the today's value of the radius R_{0a} of the Friedmann sphere using a magnitude redshift diagram of 19 SNIa.

With the help of the known values of R_{0a} and β_0 , statements about astrophysical data from the black hole in the galaxy M87 can be made. In addition, the today's Hubble parameter H_0 results from both parameters.

Furthermore, we calculate the values of the further physical redshift distances for the black hole in M87 and all 19 SNIa.

The resulting parameter values are: $\beta_0 \approx 0.731$, $R_{0a} \approx 2,712.48$ Mpc and $H_0 \approx 65.638$ km / (s · Mpc). The today's mass density of the Friedmann sphere is $\rho_0 \approx 4.843 \times 10^{-27}$ g / cm³. For the mass of the Friedmann sphere we find $M_{FK} \approx 1.206 \times 10^{56}$ g.

Annotation:

Knowledge of the first part [1] of the series of articles is a prerequisite for understanding this article.

Key words: relativistic astrophysics, theoretical and observational cosmology, redshift, Hubble parameter, quasar, black hole, SNIa, M87

PACS NO:

¹ steffen_haase@vodafone.de

Contents

1.	For Recall	3
2.	Derivation of further physical redshift distances	3
3.	Determination of the parameter values	7
3.1	Magnitude-redshift relation	7
3.2	Number-redshift relation	11
3.3	Angular size-redshift relation	12
3.4	Fixing of R_{0a} with the help of SNIa	13
3.5	Calculation of the further redshift distances for the SNIa and M87	15
3.6	Evaluation of the data from the black hole in M87	17
3.7	Maximum values known today: Galaxy UDFj-39546284 and Quasar J0313	19
4.	Final considerations.....	20
4.1	Hubble parameter	20
4.2	Mean values	23
5.	Concluding remarks	24
6.	Appendix	24

List of Figures

- Figure 1.** Redshift distance R_{ea} normalized to the distance R_{0a}
- Figure 2.** Redshift distance R_{0e} normalized to the distance R_{0a} for various values of the parameter β_0
- Figure 3.** Redshift distance R_{ee} normalized to the distance R_{0a} for different values of the parameter β_0
- Figure 4.** Today's (t_0) redshift distance D_0 normalized to the distance R_{0a} for various values of the parameter β_0
- Figure 5.** The at that time (t_e) redshift distance D_e normalized to the distance R_{0a} for various values of the parameter β_0
- Figure 6.** Magnitude-redshift diagram for all 132,975 quasars according to M.-P. Véron-Cetty et al. [2].
- Figure 7.** Magnitude-redshift diagram of the mean values $\langle z_i \rangle$ and $\langle m_i \rangle$ with inserted standard deviations σ_{m_i} and σ_{z_i}
- Figure 8.** Magnitude-redshift diagram for 132,975 quasars according to M.-P. Véron-Cetty et al. [2]
- Figure 9.** Standard deviations σ_{m_i} as a function of $\langle z_i \rangle$
- Figure 10.** Number-redshift diagram for the 132,975 quasars according to M.-P. Véron-Cetty et al. [2]
- Figure 11.** Angular size-redshift diagram according to K. Nilsson et al. [3]
- Figure 12.** Magnitude-redshift diagram for 27 SNIa according to W. L. Freedman et al. [4]
- Figure 13.** Redshift distance D (light path) and the further redshift distances D_i ($i = 0, e$) and R_{jk} ($j = 0, e; k = e, a$) as a function of the redshift up to $z = 11$
- Figure 14.** Visualization of the distances D_i , D and R_{jk} with regard to M87 and observer
- Figure 15.** All distances D_i and D for M87, J0313 and UDFj-39546284
- Figure 16.** Non-approximated redshift distance D compared to the linear Hubble redshift distance

List of Tables

- Table 1.** Redshift distance D and the further redshift distances D_i and R_{jk} of all 27 SNIa
- Table 2.** Summary of data from galaxy M87 with the black hole in it
- Table 3.** Redshift distances D_i , D and R_{jk} from the black hole in M87
- Table 4.** All calculated redshift distances R_{jk} , D_i and D for the two cosmic objects with the maximum redshifts
- Table 5.** Expansion-related shifts in the distance of the quasar and the galaxy.
- Table 6.** Various distances $R_{0a,i}$ of the 27 SNIa $_i$ calculated using the distance modules μ_i
- Table 7.** Mean values from the Quasar data set used according to [2]
- Table 8.** Numbers N_i summed up in the redshift intervals z_i of the quasars according to [2]
- Table 9.** Summary of the data which we used from the 27 SNIa according to [4]

1. For Recall

Based on the physical approach for the dynamic path of photons (light path) through the universe

$$D = a_0 r_a - a_e r_e = R_{0a} - R_{ee} \quad (I, 15)$$

we found in the first part of the series of articles [1] for the non-approximated redshift distance

$$D(z; R_{0a}, \beta_0) = \frac{R_{0a}}{(1+z)} \left[\frac{1}{\beta_0} \left(1 - \frac{1}{\sqrt{1+z}} \right) + z \right] . \quad (I, 31)$$

In the above equation, R_{0a} is the physical distance of any observer from a coordinate origin ($r = 0$).

In this paper we designate all distances that are related to a coordinate origin with "R" and all differences of such distances with "D".

For the relations relevant in the context of cosmology, we found the magnitude-redshift relation in Part I of the essay series with the help of the redshift distance

$$m(z; m_{0a}, \beta_0) = 5 \log_{10} \left[\frac{1}{\beta_0} \left(1 - \frac{1}{\sqrt{1+z}} \right) + z \right] - 5 \log_{10}(1+z) + m_{0a} , \quad (I, 38)$$

the angular size-redshift relation

$$\varphi(z; \delta / R_{0a}, \beta_0) = \frac{\delta}{R_{0a}} \frac{(1+z)}{\left[\frac{1}{\beta_0} \left(1 - \frac{1}{\sqrt{1+z}} \right) + z \right]} , \quad (I, 40)$$

and the number-redshift relation

$$\log_{10} N(z; N_{0a}, \beta_0) = 3 \log_{10} \left[\frac{1}{\beta_0} \left(1 - \frac{1}{\sqrt{1+z}} \right) + z \right] - 3 \log_{10}(1+z) + \log_{10} N_{0a} . \quad (I, 46)$$

In the following chapter we calculate further physical redshift distances related to the coordinate origin and differences of these distances that are very interesting for cosmology.

2. Derivation of further physical redshift distances

The starting point for the derivation of the further redshift distances are the elementary equations

$$(1+z) = \frac{a_0}{a_e} \quad (I, 20a) \quad \text{and} \quad D = R_{0a} - R_{ee} \quad (I, 15) \quad (1)$$

$$\text{and} \quad (1+z) = \frac{a_0 r_a}{a_e r_e} = \frac{R_{0a}}{R_{ea}} \quad \text{and} \quad (1+z) = \frac{a_0 r_e}{a_e r_e} = \frac{R_{0e}}{R_{ee}} .$$

This results in the following distances

$$\begin{aligned}
R_{ee} &= R_{0a} - D & \text{and} & & R_{ea} &= \frac{R_{0a}}{(1+z)} \\
\text{and} & & R_{0e} &= (1+z)R_{ee} & &= (1+z)(R_{0a} - D) \quad .
\end{aligned} \tag{2}$$

R_{ee} is the then distance between the galaxy emitting the light and the origin of the coordinates - at the time t_e the light was emitted.

R_{ea} is the distance of the observer's galaxy from the origin of the coordinates at that time.

R_{0e} is the today's - at time t_0 , at which the light is absorbed by the observer - distance of the light-emitting galaxy from the origin of the coordinates.

R_{0a} is today's distance of the galaxy containing the observer from the origin of the coordinates.

These distances become concretely with equation (I, 31)

$$R_{ee}(z; R_{0a}, \beta_0) = R_{0a} \left\{ 1 - \frac{1}{(1+z)} \left[\frac{1}{\beta_0} \left(1 - \frac{1}{\sqrt{1+z}} \right) + z \right] \right\} \tag{3}$$

and

$$R_{0e}(z; R_{0a}, \beta_0) = R_{0a} \left[1 - \frac{1}{\beta_0} \left(1 - \frac{1}{\sqrt{1+z}} \right) \right] \tag{4}$$

and of course too

$$R_{ea}(z; R_{0a}) = \frac{R_{0a}}{(1+z)} \quad . \tag{5}$$

These distances from the coordinate origin result

$$D_e(z; R_{0a}, \beta_0) = \frac{R_{0a}}{\beta_0} \frac{\left(1 - \frac{1}{\sqrt{1+z}} \right)}{(1+z)} \quad . \tag{6}$$

D_e is the then (t_e) distance between the observed galaxy and the galaxy in which the observer is located.

Furthermore we find

$$D_0(z; R_{0a}, \beta_0) = \frac{R_{0a}}{\beta_0} \left(1 - \frac{1}{\sqrt{1+z}} \right) \quad . \tag{7}$$

D_0 is the today's distance between the two participating galaxies.

The following figures illustrate the equations for the further redshift distances, where we have normalized all distances to R_{0a} .

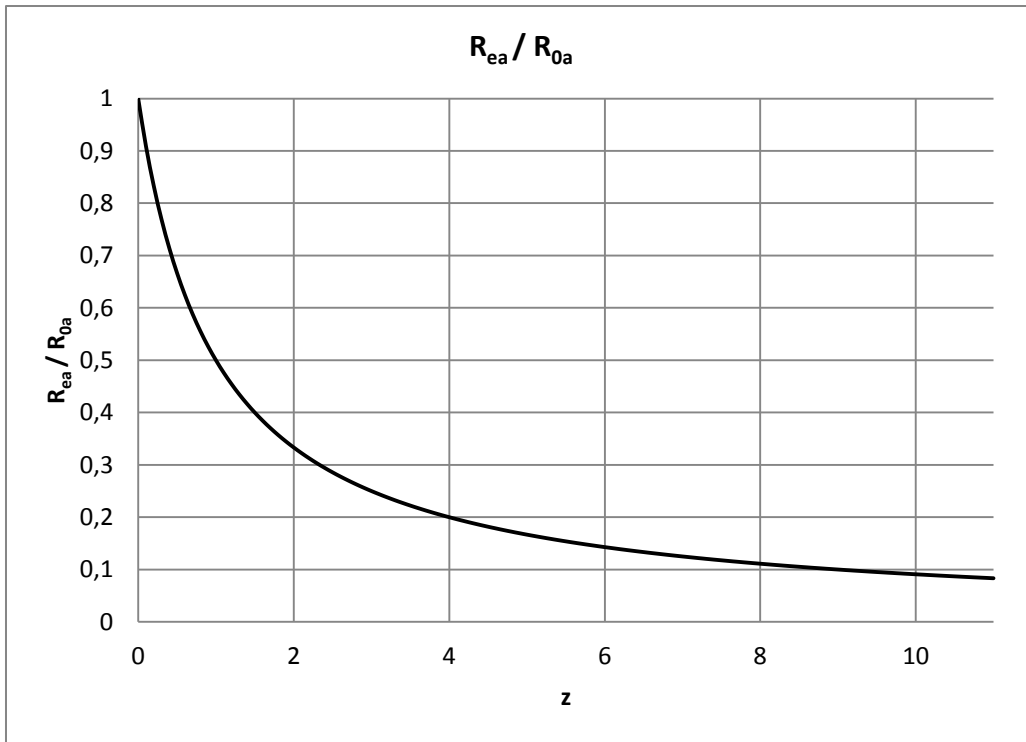


Figure 1. Redshift distance R_{ea} normalized to the distance R_{0a} .

This distance does not depend on the parameter β_0 .

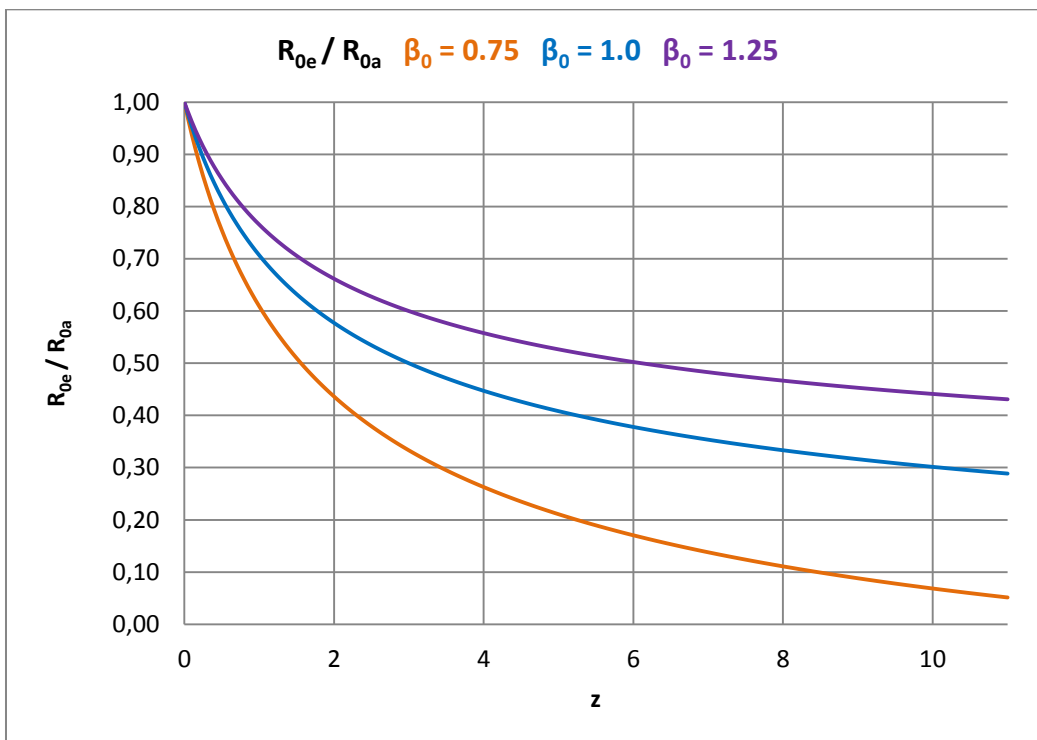


Figure 2. Redshift distance R_{0e} normalized to the distance R_{0a} for various values of the parameter β_0 .

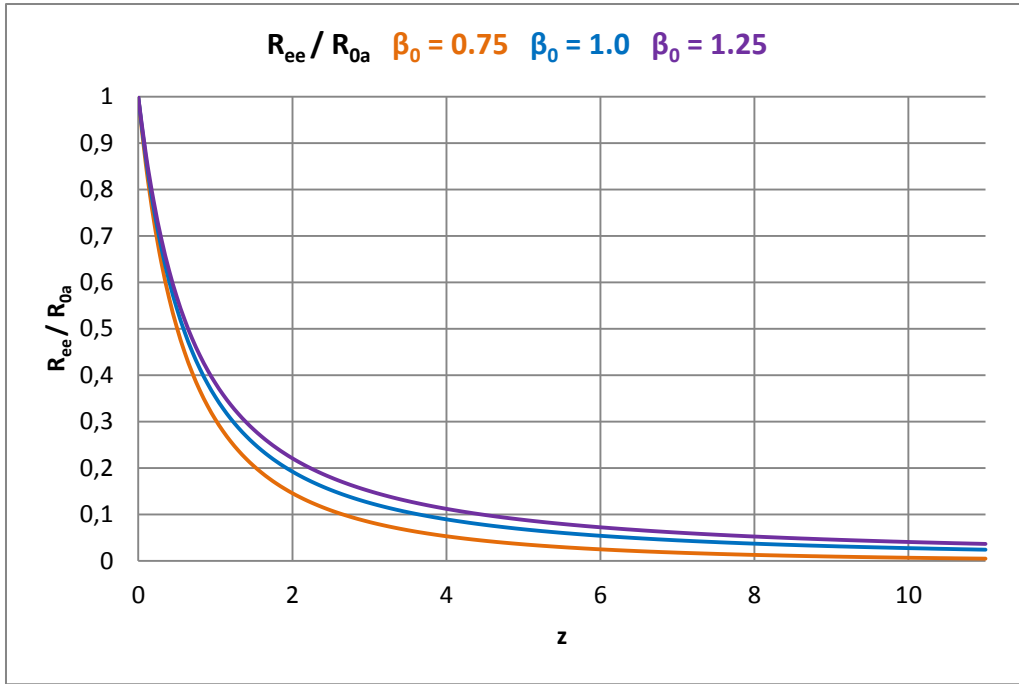


Figure 3. Redshift distance R_{ee} normalized to the distance R_{0a} for different values of the parameter β_0 .

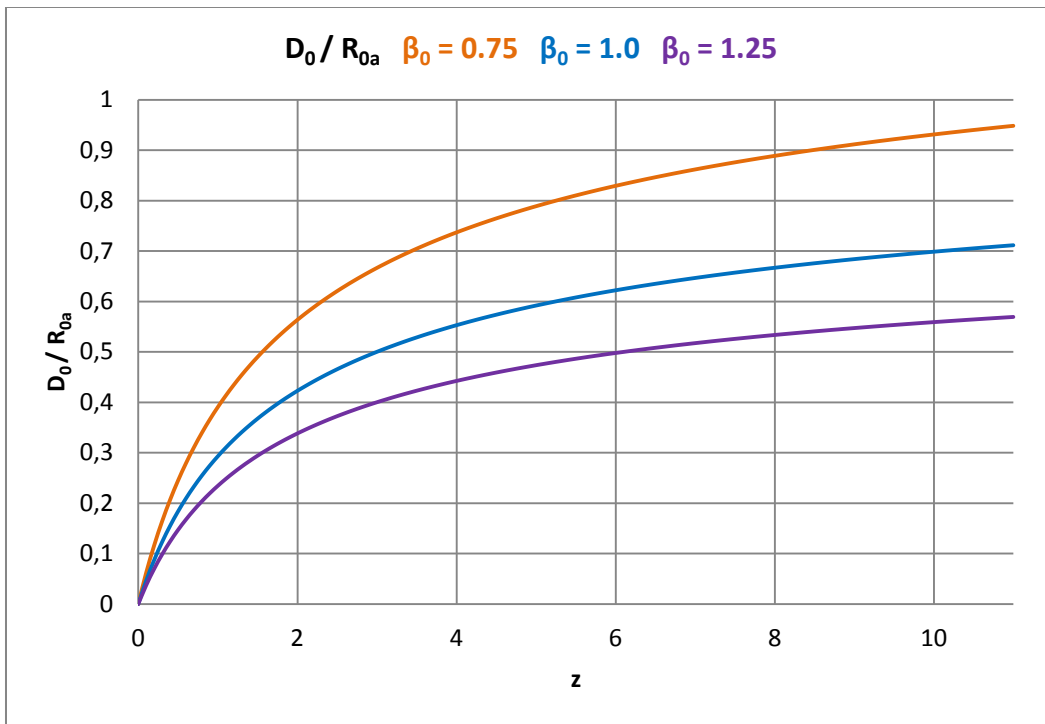


Figure 4. Today's (t_0) redshift distance D_0 normalized to the distance R_{0a} for various values of the parameter β_0 .

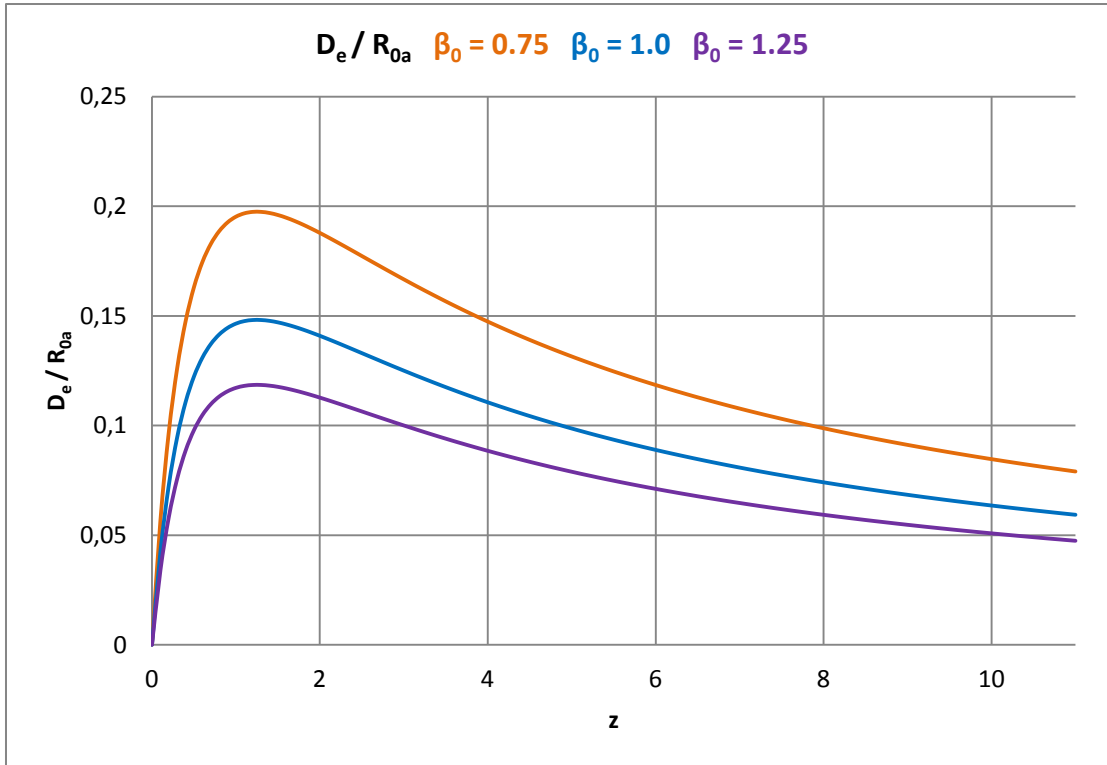


Figure 5. The at that time (t_e) redshift distance D_e normalized to the distance R_{0a} for various values of the parameter β_0 .

In the specialist literature, none of these redshift distances are known and they cannot be derived there, respectively.

We will give concrete values for these redshift distances for the galaxy M87 and 27 SNIa below.

3. Determination of the parameter values

3.1 Magnitude-redshift relation

The apparent magnitude m depends according to Eq. (I.38) in addition to the measurable redshift z also on the parameters β_0 and m_{0a} .

To find both parameters, the quasar catalog by Véron-Cetty [2] is suitable in which measured redshifts and apparent magnitudes of 132,975 quasars are given.

Fig. 6 shows all these quasars in a single magnitude-redshift diagram, where we have used $\log_{10}(cz)$ as the abscissa.

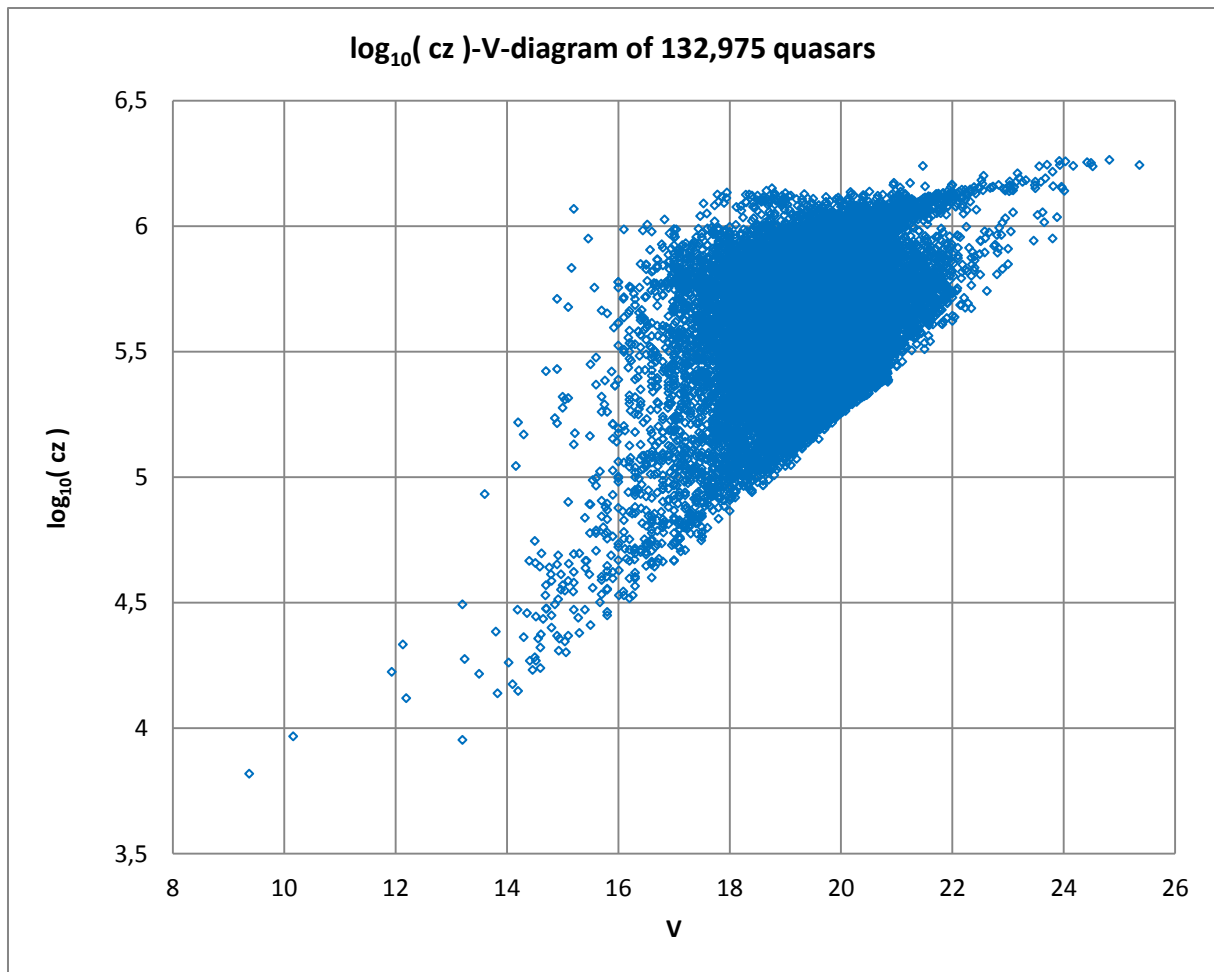


Figure 6. Magnitude-redshift diagram for all 132,975 quasars according to M.-P. Véron-Cetty et al. [2].

A clear edge can be seen on the right side of the accumulation of measurement points, which indicates minimum apparent magnitudes for associated redshifts. The apparent magnitudes are usually up to far to the left of this edge in the diagram.

If we form redshift intervals with mean values of the redshifts and the corresponding mean values for the apparent magnitude, this fact leads to a clear curvature of the mean value curve in the direction of the redshift axis.

The quasars cannot therefore be described in the diagram by a linear curve. This suggests that our redshift distance [i.e. ultimately Eq. (I, 38)] could be suitable for the measured values.

It is precisely this strange magnitude-redshift diagram that has stimulated us to think about cosmological distance determinations for many years [10].

To evaluate the quasar data set, we first create 75 z-intervals with 1,773 quasars each. For these intervals we calculate the mean values $\langle z_i \rangle$ and the associated mean values $\langle m_i \rangle$ of the quasars. For all intervals we also calculate the standard deviations $\sigma_{m,i}$ and also the standard deviations $\sigma_{z,i}$. The latter, however, do not play a role in the analysis of the data set. The appendix contains the associated table, which also contains all $\sigma_{m,i}$.

Figure 7 shows the magnitude-redshift diagram after averaging with all of the standard deviations $\sigma_{m,i}$ and $\sigma_{z,i}$ calculated by us.

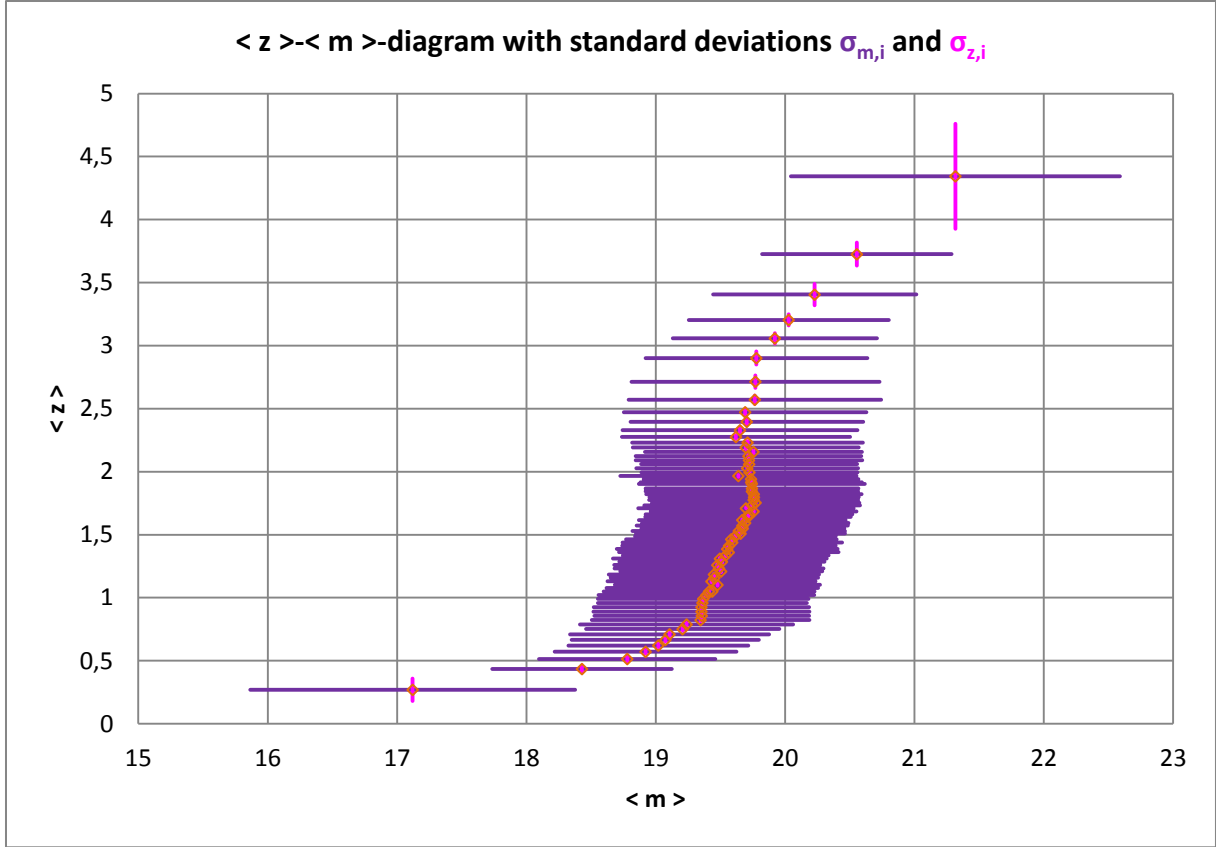


Figure 7. Magnitude-redshift diagram of the mean values $\langle z_i \rangle$ and $\langle m_i \rangle$ with inserted standard deviations $\sigma_{m,i}$ and $\sigma_{z,i}$.

The curvature of the curve expected on the basis of Figure 6 can be clearly seen. This curvature should be explained by means of theory. More precisely: The theory has to explain the curvature!

We use the likelihood function

$$\chi^2(p_k) = \sum_{i=1}^N \frac{[m_{th,i}(p_k) - m_{obs,i}]^2}{\sigma_{m,i}^2} \quad (8)$$

for the evaluation.

p_k with $k = 1, 2$ stands for the two parameters we are looking for, β_0 and m_{0a} .

If we use our magnitude-redshift relation (I, 38), the result is concrete

$$\chi^2(\beta_0, m_{0a}) = \sum_{i=1}^N \frac{\left[5 \log_{10} \left[\frac{1}{\beta_0} \left(1 - \frac{1}{\sqrt{1+z_i}} \right) + z_i \right] - 5 \log_{10}(1+z_i) + m_{0a} - m_{obs,i} \right]^2}{\sigma_{m,i}^2} \quad (8a)$$

Using the quasar data and using the usual mathematical procedure, we can find the parameters $\beta_0 = 0.7311668$ and $m_{0a} = 20.1346$.

Figure 8 shows the result of the mean value formation and the adaptation of the theory to the curvature of the mean value curve.

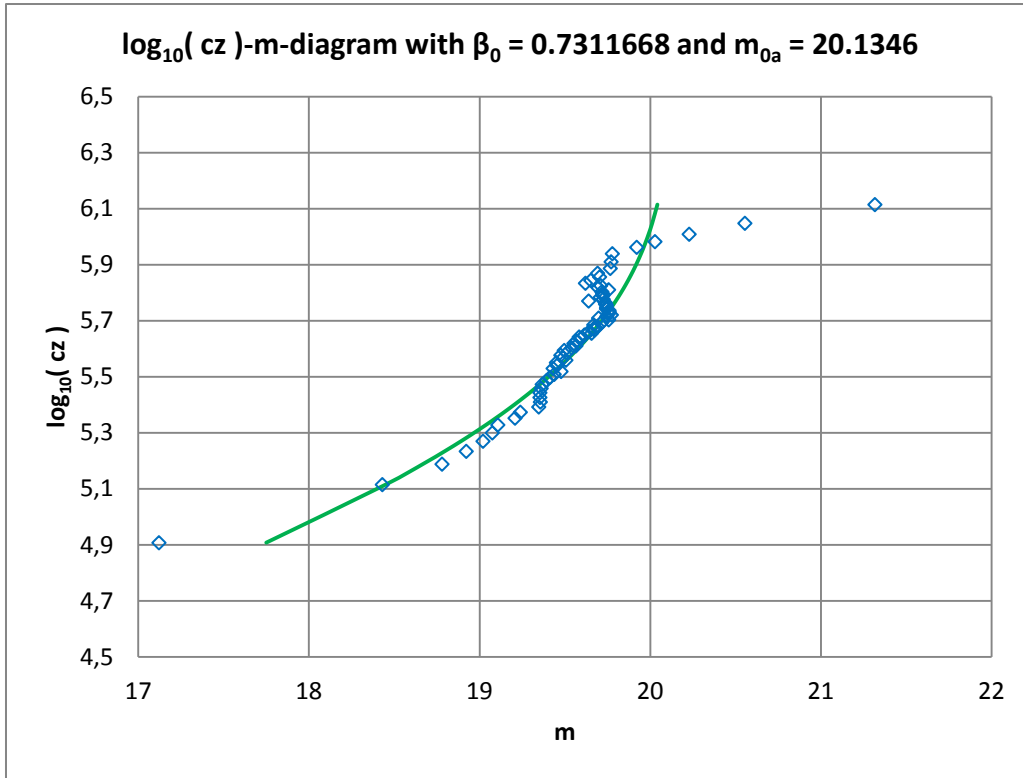


Figure 8. Magnitude-redshift diagram for 132,975 quasars according to M.-P. Véron-Cetty et al. [2].

For comparison:

In Part I of the series of articles we found the somewhat larger value $m_{0a} \approx 20.24$ of today's apparent limit magnitude for much fewer quasars under the justified assumption of $\beta_0 = 1$. There, this value for β_0 best describes the curvature of the measured value curve for large redshifts.

To interpret the measured magnitude-redshift relation:

From our point of view, the quasars came in to being historically slowly as relatively weakly luminous objects at a point in time that corresponds to about $z \approx 4.3$. The quasars later behaved as the theory expects in flat space and moved with time - i.e. for decreasing redshifts z - on average along the theoretical curve (in the diagram from top right diagonally to bottom left). The quasars have gradually died out in the recent past and have become relatively bright in the process.

The dependence of the calculated standard deviations $\sigma_{m, i}$ on the redshift mean values $\langle z_i \rangle$ is shown in Figure 9.

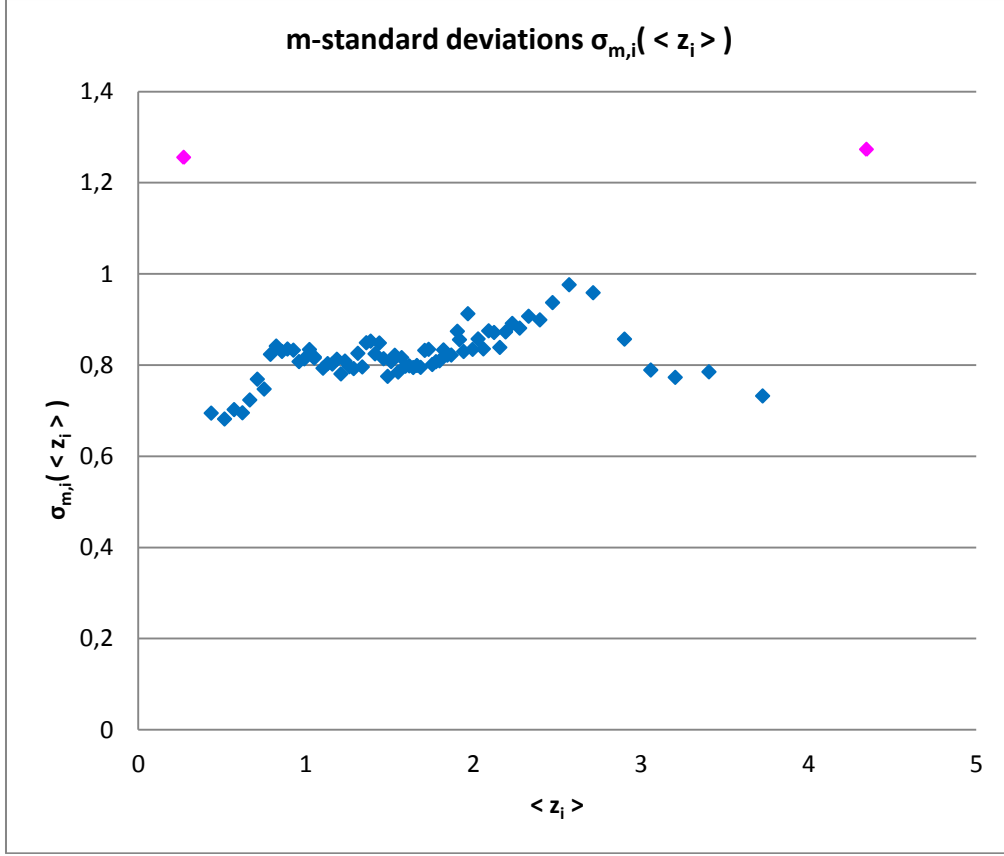


Figure 9. Standard deviations $\sigma_{m,i}$ as a function of $\langle z_i \rangle$.

If we consider the first and last point in the diagram as outliers and therefore simply do not take them into account when evaluating the magnitude-redshift diagram of the quasars, we find the parameters $\beta_0 = 0.5486497$ and $m_{0a} = 19.9555$ for the values.

Because of the differences to the values mentioned above, we might come up with the idea of taking the mean values of each of these. But we will not do that in the following.

3.2 Number-redshift relation

We use the following variance to evaluate the number-redshift relation

$$\chi^2(p_k) = \frac{1}{N-1} \sum_{i=1}^N [N_{th,i}(p_k) - N_{obs,i}]^2 \quad . \quad (9)$$

p_k with $k = 1, 2$ stands for the two parameters we are looking for, β_0 and N_{0a} .

If we insert our number-redshift relation (I, 46), the result is concrete

$$\chi^2(\beta_0, N_{0a}) = \frac{1}{N-1} \sum_{i=1}^N \left\{ 3 \log_{10} \left[\frac{1}{\beta_0} \left(1 - \frac{1}{\sqrt{1+z_i}} \right) + z \right] - 3 \log_{10}(1+z_i) + \log_{10} N_{0a} - N_{obs,i} \right\}^2 \quad . \quad (9a)$$

Using simple mathematics, we find $N_{0a} = 146,816$ for the theoretically expected total number of quasars, if we use the value $\beta_0 = 0.7311668$ found via the magnitude-redshift relation.

The expected number is slightly larger than the actual number of quasars measured. This indicates a certain incompleteness of the measurements.

Figure 10 shows the graphic result.

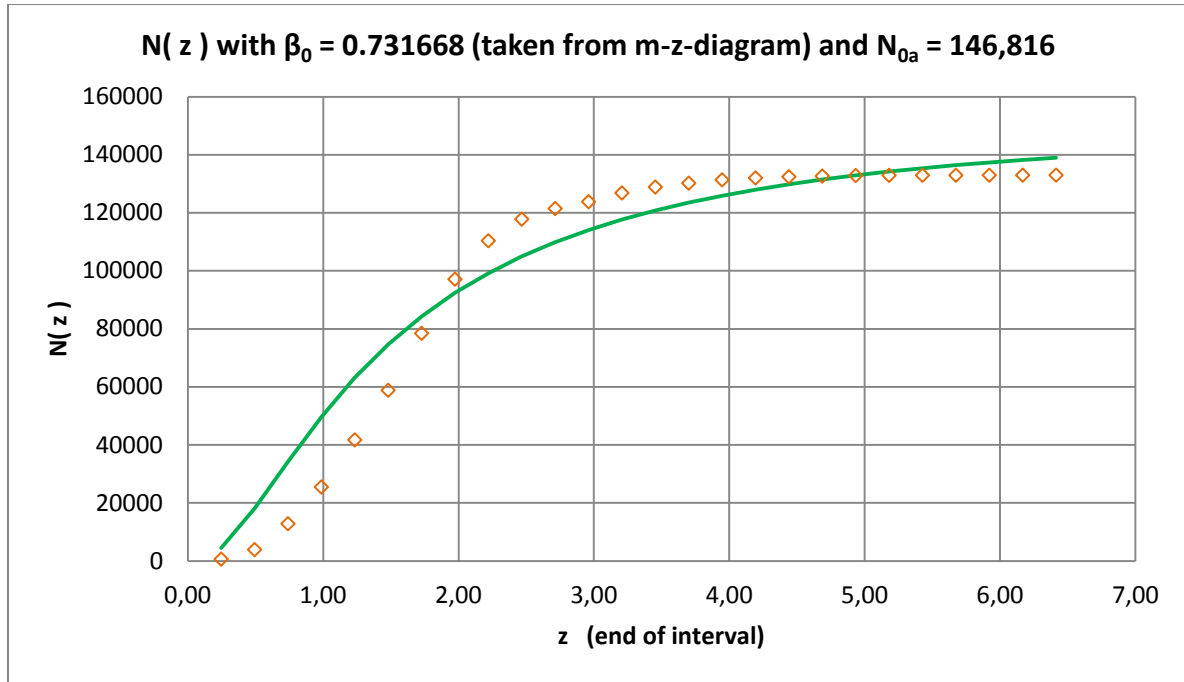


Figure 10. Number-redshift diagram for the 132,975 quasars according to M.-P. Véron-Cetty et al. [2].

Another possibility is to determine both parameters directly via the number-redshift relation, i.e. not to use the value of β_0 from the magnitude-redshift diagram of the quasars. This leads to the parameter values $N_{0a} = 159,140$ and $\beta_0 = 0.8653211$. Both values are slightly larger than those noted above.

Overall, we could build a mean value using three different values of β_0 . However, we will not make use of this in the following.

3.3 Angular size-redshift relation

As in Part I, we use the measurement data from K. Nilsson et al. [3] to find an average linear size of the cosmic objects measured there.

The starting point is the variance

$$\chi_{\varphi}^2(p_k) = \frac{1}{N-1} \sum_{i=1}^N [\varphi_{th,i}(p_k) - \varphi_{obs,i}]^2 \quad . \quad (10)$$

Here, p_k with $k = 1, 2$ stands for the two parameters we are looking for, β_0 and δ / R_{0a} .

If we use our angular size-redshift relation (I, 40), the result is concrete

$$\chi_{\varphi}^2\left(\frac{\delta}{R_{0a}}, \beta_0\right) = \frac{1}{N-1} \sum_{i=1}^N \left\{ \frac{\delta}{R_{0a}} \frac{(1+z)}{\left[\frac{1}{\beta_0} \left(1 - \frac{1}{\sqrt{1+z}} \right) + z \right]} - \varphi_{obs,i} \right\}^2 \quad . \quad (10a)$$

The comparison of the theory with the measurement data using $\beta_0 = 0.7311668$ results in a value of $\delta / R_{0a} = 6.06 \times 10^{-5}$.

Figure 11 shows the graphic result.

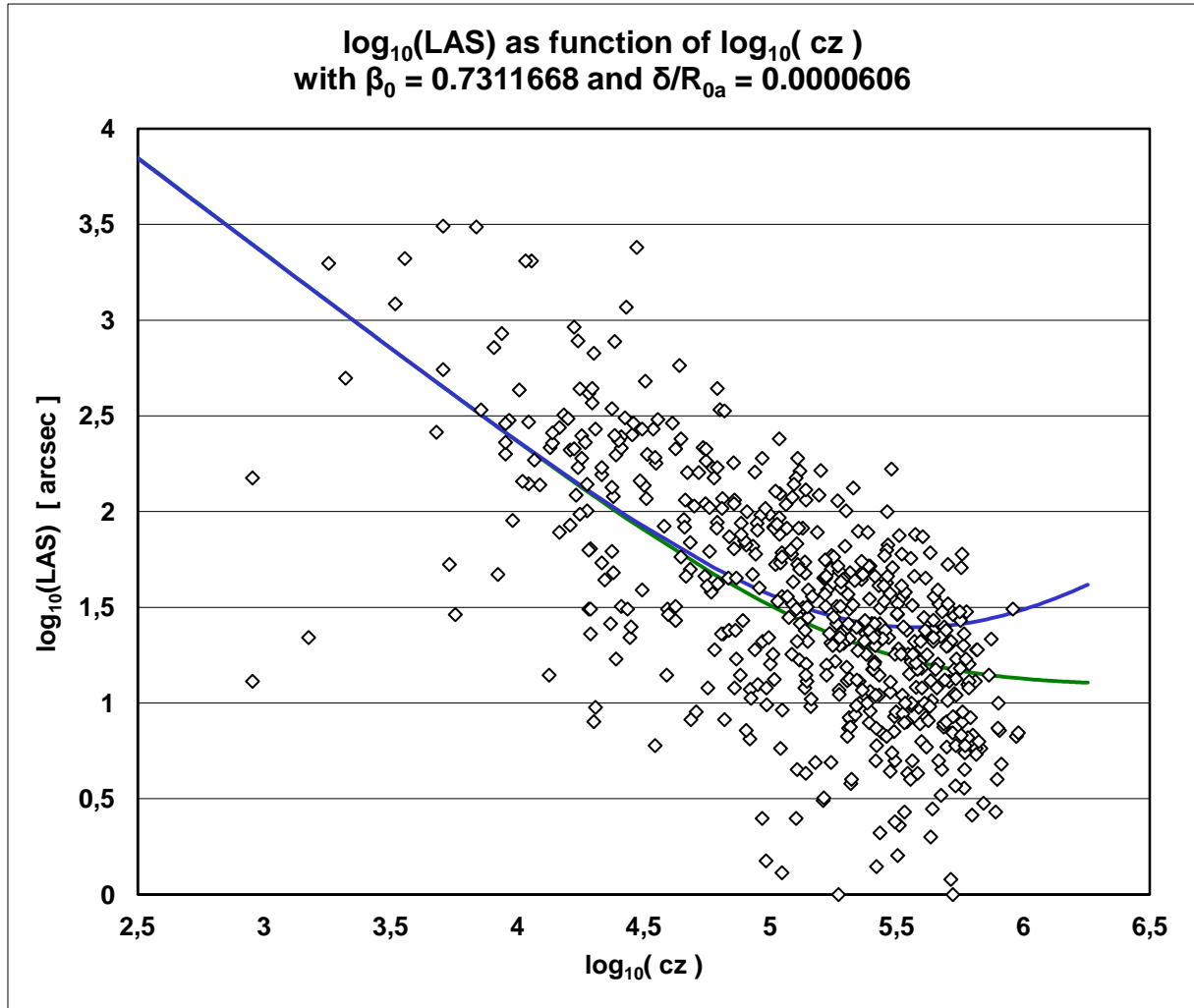


Figure 11. Angular size-redshift diagram according to K. Nilsson et al. [3].

For the purpose of comparison, the theoretical curve from the literature was drawn in (see Part I). This curve cannot explain the position of the measured values in the diagram.

The determination of the linear size δ requires the knowledge of R_{0a} . Because the absolute magnitudes are known for some SNIa (which differ slightly from one another), we can determine R_{0a} using a magnitude-redshift diagram of these objects. We'll do that in the next chapter.

3.4 Fixing of R_{0a} with the help of SNIa

By W. L. Freedman et al. [4], data from a total of 27 SNIa were made available, with the help of which we can determine both the distance R_{0a} - a current distance - and, as a result, the today's Hubble parameter H_0 . The data we are interested in are the distance modules (μ_{TRGB} and μ_{Ceph}), the maximum apparent magnitudes (m_{CSP_B0} and m_{SC_B}) and the radial velocities V_{NED} , from which the redshifts z_{NED} can be calculated. The methods taken into account in [4] for determining the maximum apparent magnitude and thus the associated absolute magnitude are different, which is why somewhat different values are given for one and the same SNIa. For our purposes, we calculate the mean values from these data and assign them to the relevant SNIa.

We calculate the absolute magnitudes M_i of the SNIa_i using $(\mu_{\text{TRGB}} - m_{\text{CSP}_B0})$ and $(\mu_{\text{Ceph}} - m_{\text{SC}_B})$ and then always calculate an average value $\langle M_i \rangle$ if both value pairs are specified for one and the same SNIa. From all the absolute magnitudes obtained in this way, we finally form the mean value of the absolute magnitude $\langle M \rangle \approx -19.245$, which enables us to determine the distance R_{0a} with the aid of the parameter m_{0a} , which results from the magnitude-redshift diagram of the SNIa. The simple equation for this is

$$R_{0a} = 10^{\frac{m_{0a} - M}{5} + 1} . \quad (\text{I,47})$$

The graphic result is shown in Figure 12.

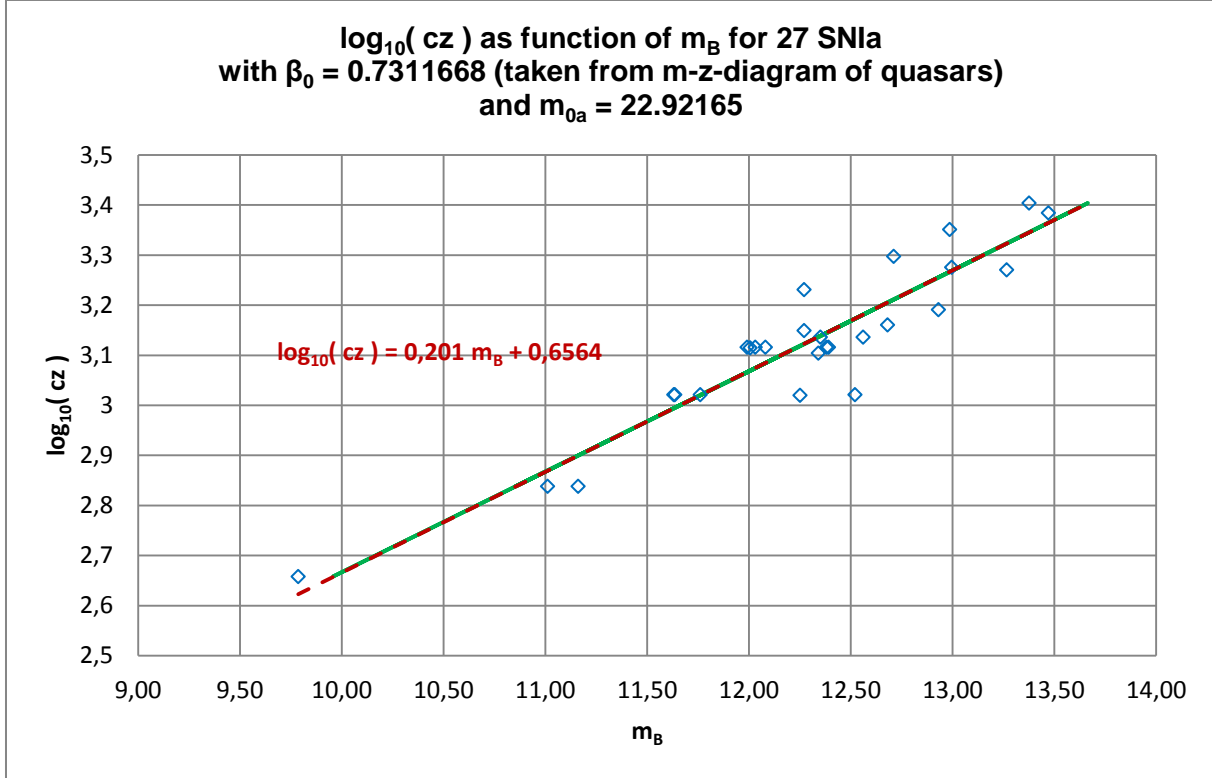


Figure 12. Magnitude-redshift diagram for 27 SNIa according to W. L. Freedman et al. [4].

The theoretical curve lies exactly on the linear trend line (dashed in red), the equation of which is given in the figure.

Using $m_{0a} \approx 22.922$ and the mean value of the absolute brightness $\langle M \rangle = -19.245$, the distance $R_{0a} \approx 2,712.48$ Mpc we are ultimately looking for is the essential result of this data analysis.

With the help of the value of R_{0a} and using the equation (an approximation for small redshifts!)

$$H_{0a} \approx \frac{c}{\left(\frac{1}{2\beta_0} + 1 \right) R_{0a}} \quad (\text{I,34})$$

the today's Hubble parameter $H_0 \approx 65.638 \text{ km} / (\text{s} \cdot \text{Mpc})$ results. This value is slightly below the Planck value (2018) with $H_{0, \text{Planck}} \approx 67.66 \text{ km} / (\text{s} \cdot \text{Mpc})$ [5].

In Table 8 in the appendix, all the values we used for the magnitude-redshift diagram of the 27 SNIa are compiled.

Starting from the equation

$$\frac{1}{\beta_0} = \frac{2c}{R_{0a} \sqrt{\frac{8\pi G \rho_0}{3}}} \quad (I,30)$$

equation (11) results for today's mass density:

$$\rho_0 = \frac{3}{2\pi} \frac{c^2}{G} \frac{\beta_0^2}{R_{0a}^2} \quad (11)$$

With the theoretical parameters β_0 and R_{0a} determined by us, we find $\rho_0 \approx 4.843 \times 10^{-27} \text{ g/cm}^3$ for today's matter density in the universe.

Via

$$M_{FK} = \frac{4\pi}{3} R_{0a}^3 \rho_0 = \frac{4\pi}{3} R_{0a}^3 \frac{3}{2\pi} \frac{c^2}{G} \frac{\beta_0^2}{R_{0a}^2} \quad i.e. \quad M_{FK} = \frac{2c^2}{G} \beta_0^2 R_{0a} \quad (12)$$

the constant mass of the Friedmann sphere results in $M_{FK} \approx 1.206 \times 10^{56} \text{ g}$.

Because we generally do not consider the accuracy here, we simply specify the decimal places with up to 3 places, whereby the mathematical analysis of the data usually delivers more decimal digits.

With the known value $R_{0a} \approx 2,712.48 \text{ Mpc}$ we can calculate the mean linear size of the Nilsson objects [3] to be $\delta \approx 0.164 \text{ Mpc}$, because we have found $\delta / R_{0a} = 6.06 \times 10^{-5}$ for them.

Using R_{0a} and β_0 , of course, all linear dimensions of these objects can be calculated using their angular size and redshift.

3.5 Calculation of the further redshift distances for the SNIa and M87

Because we were able to determine R_{0a} , we can graphically display the further redshift distances in a form that is not normalized to R_{0a} . The result is shown in Figure 13, using the values we found for β_0 and R_{0a} .

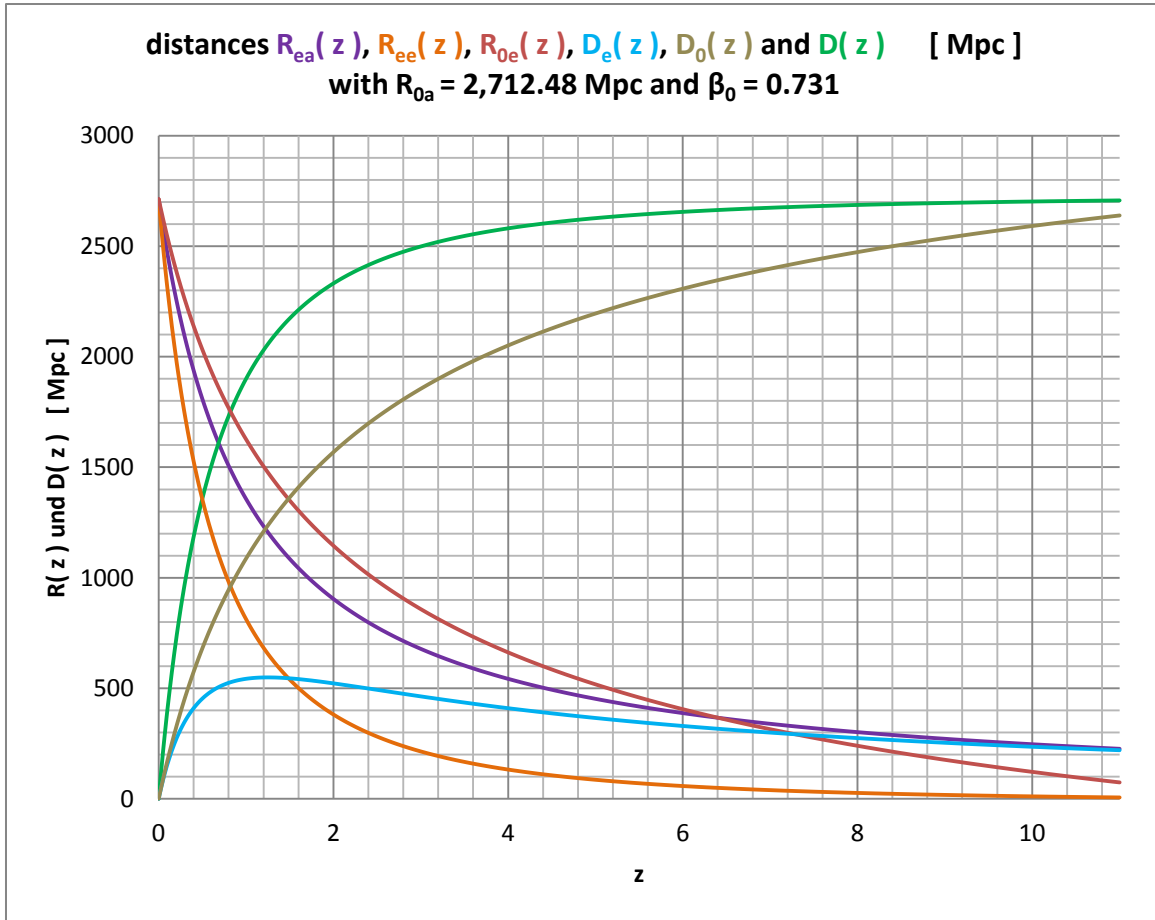


Figure 13. Redshift distance D (light path) and the further redshift distances D_i ($i = 0, e$) and R_{jk} ($j = 0, e; k = e, a$) as a function of the redshift up to $z = 11$.

For the representation we have chosen $z \leq 11$, because currently no cosmic objects with larger measured redshifts are known.

To interpret Figure 13:

a) For $D \rightarrow R_{0a}$ the redshift z goes towards infinity. This means that no observer can observe objects for which is $D \geq R_{0a} \approx 2,712.48$ Mpc.

b) As already mentioned in Part I, the light path distance $D = R_{0a} - R_{ee}$ is always greater than the distance differences D_0 (today) and D_e (then).

In particular, the light path D is not equal to the today's distance D_0 between the two astrophysical objects.

c) The distances R_{jk} are physical distances from a coordinate origin and develop directly with the change in the scale parameter $a(t)$ over time. For large redshifts, the scale parameter was correspondingly small and, as a result, the associated distances were also correspondingly small.

d) The distance D_e at that time is interesting: It shows a maximum for a specific redshift and only approaches zero for very large redshifts. This is also the reason for the further approximation of D_0 to D only for very large redshifts.

Table 1 summarizes all calculated redshift distances of the 27 SNIa.

SNIa	R_{ea}	R_{ee}	R_{0e}	R_{0a}	D_e	D_0	D
1980N	2,700.72	2,692.70	2,704.43	2,712.48	8.02	8.05	19.78
1981B	2,703.02	2,696.56	2,706.00	2,712.48	6.46	6.48	15.92
1981D	2,700.72	2,692.70	2,704.43	2,712.48	8.02	8.05	19.78
1989B	2,706.26	2,702.02	2,708.23	2,712.48	4.25	4.26	10.47
1990N	2,703.02	2,696.56	2,706.00	2,712.48	6.46	6.48	15.92
1994D	2,703.02	2,696.56	2,706.00	2,712.48	6.46	6.48	15.92
1994ae	2,698.51	2,689.00	2,702.92	2,712.48	9.52	9.57	23.49

1995al	2,695.53	2,683.98	2,700.87	2,712.48	11.54	11.61	28.50
1998aq	2,700.16	2,691.76	2,704.05	2,712.48	8.40	8.44	20.72
1998bu	2,706.26	2,702.02	2,708.23	2,712.48	4.25	4.26	10.47
2001el	2,703.04	2,696.60	2,706.02	2,712.48	6.44	6.46	15.88
2002fk	2,695.72	2,684.31	2,701.00	2,712.48	11.41	11.48	28.17
2003du	2,690.74	2,675.97	2,697.59	2,712.48	14.78	14.90	36.51
2005cf	2,692.33	2,678.63	2,698.68	2,712.48	13.70	13.81	33.86
2006dd	2,700.72	2,692.70	2,704.43	2,712.48	8.019	8.054	19.78
2007af	2,694.66	2,682.53	2,700.27	2,712.48	12.13	12.21	29.95
2007on	2,700.72	2,692.70	2,704.43	2,712.48	8.02	8.05	19.78
2007sr	2,697.17	2,686.74	2,702.00	2,712.48	10.43	10.49	25.74
2009ig	2,689.75	2,674.30	2,696.90	2,712.48	15.45	15.58	38.18
2011by	2,700.16	2,691.76	2,704.05	2,712.48	8.40	8.44	20.72
2011fe	2,708.37	2,705.56	2,709.67	2,712.48	2.81	2.81	6.92
2011iv	2,700.72	2,692.70	2,704.43	2,712.48	8.02	8.05	19.78
2012cg	2,703.02	2,696.56	2,706.00	2,712.48	6.46	6.48	15.92
2012fr	2,700.75	2,692.76	2,704.45	2,712.48	7.99	8.03	19.72
2012ht	2,699.45	2,690.58	2,703.56	2,712.48	8.88	8.92	21.91
2013dy	2,699.79	2,691.13	2,703.79	2,712.48	8.65	8.69	21.35
2015F	2,701.03	2,693.23	2,704.64	2,712.48	7.81	7.84	19.26

Table 1. Redshift distance D and the further redshift distances D_i and R_{jk} of all 27 SNIa.

To interpret the distances from Table 1:

For a more detailed explanation, we take the SNIa **2006dd**, for example, and use it to interpret the meaning of the distances in the table.

The "light-travel time" always means the time interval between the emission of light (time t_e , 2006dd) by the SNIa 2006dd and today (t_0), i.e. $\Delta t = t_0 - t_e$, 2006dd. This light-travel time is generally different for all observable cosmic objects, here especially for the individual SNIa we have considered.

a) Today's (t_0) distance between the selected SNIa and us as observers is $D_0 \approx 8.054$ Mpc.

b) The then (t_e) distance between this SNIa and us as observers was $D_e \approx 8.019$ Mpc.

According to this, the distance between the two cosmic objects has increased by about 0.035 Mpc during the light-travel time $\Delta t = t_0 - t_e$, 2006dd.

c) The SNIa has been shifted expansively away from the origin of the coordinates by $\Delta R_e = R_{0e} - R_{ee} \approx 11.73$ Mpc during the light-travel time due to the time-dependent scale parameter $a(t)$.

d) The galaxy with us as observers has been expansively shifted away from the origin of the coordinates by $\Delta R_a = R_{0a} - R_{ea} \approx 17.765$ Mpc during the t light-travel time travel due to $a(t)$.

The difference between the two displacement distances is of course the increase in the distance between the two cosmic objects noted above.

e) The light path covered by the photons within the time $\Delta t = t_0 - t_e$, 2006dd (redshift distance) is $D \approx 19.78$ Mpc. It is unequal to the other mentioned distances D_i and also greater than these.

3.6 Evaluation of the data from the black hole in M87

For the sake of simplicity, we summarize the data from the literature on the galaxy M87 with the black hole (BH) in it in the first line of Table 2 {s. [6] and [7]}.

The second line lists the data specified here, which usually differ from those in the literature.

	D [Mpc]	M_B [mag]	z	m_B [mag]	Θ_{BH} [μ as]	$\delta/2 = R_S$ [pc]	M_{BH} [g]
literature	16.9 / 16.8	-23.5	0.004283	9.6	42		1.2928E+43
we	19.45	-21.84				0.227	2.3584E+45

Table 2. Summary of data from galaxy M87 with the black hole in it.

The theory was adapted to the measured angle size Θ_{BH} from the literature. Overall, a larger redshift distance D , a smaller absolute magnitude M_B and a significantly larger mass M_{BH} of the black hole follow.

Table 3 lists the values found by means of our theory for all redshift distances R_{jk} , D_i and for D .

[Mpc]	R_{ea}	R_{ee}	R_{0e}	R_{0a}	D_e	D_0	D
we	2,700.92	2,693.03	2,704.56	2,712.48	7.89	7.92	19.45
literature	---	---	---	---	---	---	16.8

Table 3. Redshift distances D_i , D and R_{jk} from the black hole in M87.

From these values, the expansion-related shifts in distance of the galaxy M87 and of the galaxy with us as observers can be calculated, which took place during the time of light travel.

The theory from the literature does not know the first 5 listed distances. It can therefore not be calculated using this theory and also not determine in terms of value.

The distance D differs because of the physical meaning: In our theory, D is the real physical light path, which is not the case in the literature.

We briefly interpret the meaning of the distances in Table 3, whereby the light-travel time is again defined as above:

- Today's (t_0) distance between the black hole (BH) or the galaxy M87 and us as observers is $D_0 \approx 7.92$ Mpc.
 - The then (t_e) distance between the BH (or M87) and us as observers was $D_e \approx 7.89$ Mpc.
- Accordingly, the distance between the two cosmic objects has increased by about 0.03 Mpc during the light-travel time $\Delta t = t_0 - t_e$, BH, M87.
- The BH (or M87) has been shifted expansively away from the origin of the coordinates by $\Delta R_e = R_{0e} - R_{ee} \approx 11.53$ Mpc during the light-travel time due to the time-dependent scale parameter $a(t)$.
 - The galaxy with us as observer was expansively shifted away from the origin of the coordinates by $\Delta R_a = R_{0a} - R_{ea} \approx 11.57$ Mpc during the light-travel time due to $a(t)$.
 - The light path (redshift distance) covered by the photons during the time $\Delta t = t_0 - t_e$, BH, M87 is $D \approx 19.45$ Mpc. It is unequal to the other mentioned distances D_i and also greater than these.

Figure 14 shows the various calculated distances in a clear form.

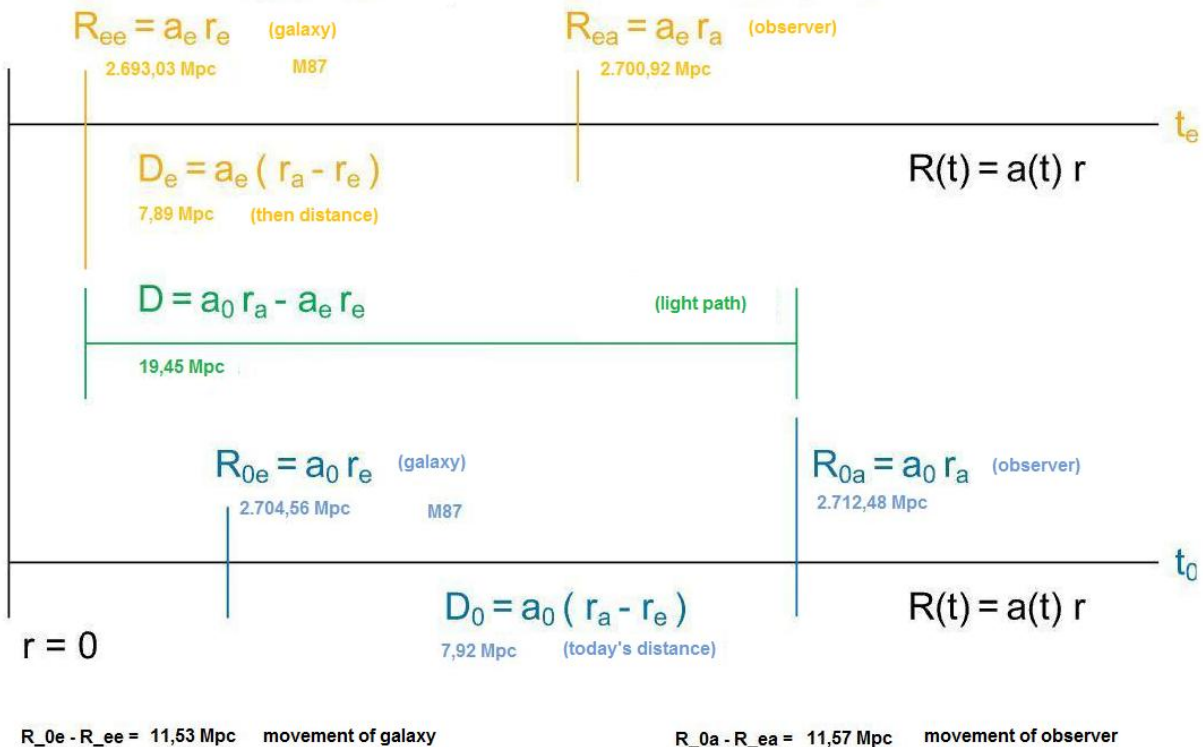


Figure 14. Visualization of the distances D_i , D and R_{jk} with regard to M87 and observer.

The distances are not drawn to scale here.

3.7 Maximum values known today: Galaxy UDFj-39546284 and Quasar J0313

The galaxy UDFj-39546284 [8] currently holds the record among the galaxies with a redshift of $z = 10.3$, while the quasar J0313 [9] with $z = 7.642$ holds the analog record among the quasars.

Table 4 shows the corresponding distances R_{jk} , D_i and D together.

object name	z	D	D_0	D_e	R_{ee}	R_{0e}	R_{ea}	R_{0a}	object
J0313	7.642	2,681.858	1,789.782	207.103	30.622	264.636	313.872	2,712.480	quasar
UDFj-39546284	10.300	2,703.075	1,905.566	168.634	9.405	106.281	240.042	2,712.480	galaxy

Table 4. All calculated redshift distances R_{jk} , D_i and D for the two cosmic objects with the maximum redshifts.

Table 5 summarizes the spatial shifts of the objects with respect to the coordinate origin due to the expansion during the associated light travel times.

object name	$R_{0e} - R_{ee}$	$R_{0a} - R_{ea}$	object
J0313	234.014	2,398.608	quasar
UDFj-39546284	96.876	2,472.438	galaxy

Table 5. Expansion-related shifts in the distance of the quasar and the galaxy.

We have already explained above how the tables are to be interpreted.

Figure 15 shows the distances D_i and D of the 3 special astrophysical objects analyzed here in a diagram, whereby we have entered all numerical values for the distances in Mpc.

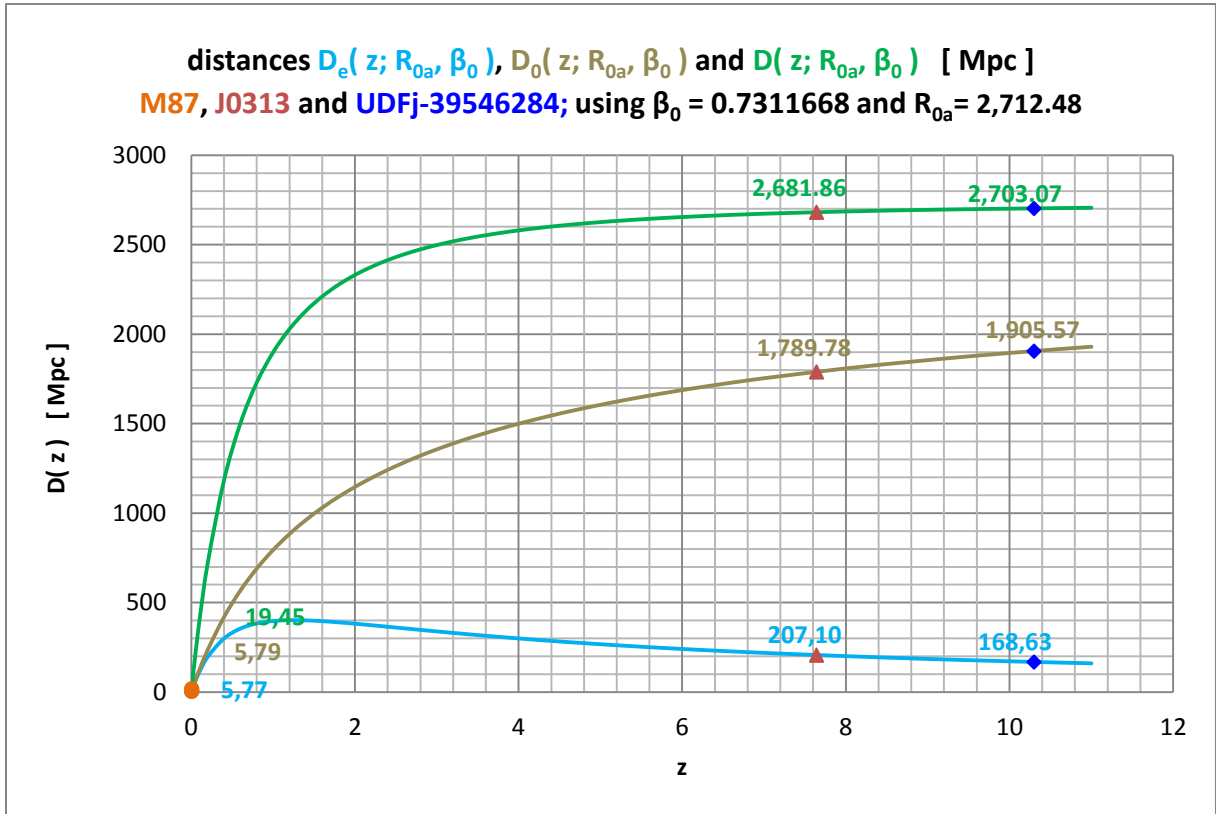


Figure 15. All distances D_i and D for M87, J0313 and UDFj-39546284.

The middle curve shows the current distances D_0 of the objects from us as observers. These distances are clearly smaller than the associated light paths D .

4. Final considerations

4.1 Hubble parameter

At this point we explicitly point out that our equation of today's Hubble parameter - which also only applies to very small redshifts - differs significantly from the definition (!) used in the literature:

$$H_{0a} \approx \frac{1}{\left(\frac{1}{2\beta_0} + 1\right)} \frac{c}{R_{0a}} \quad (we) \tag{13}$$

and

$$H_{0,lit} = \frac{\dot{a}_0}{a_0} = \frac{\dot{a}_0 r_a}{a_0 r_a} = \frac{\dot{R}_{0a}}{R_{0a}} \quad r_a = const \quad (literature) .$$

For an arbitrary point in time t this is

$$H_a(t) \approx \frac{1}{\left(\frac{1}{2\beta(t)} + 1\right)} \frac{c}{a(t)r_a} = \frac{1}{\left[\sqrt{\frac{a(t)r_a}{R_s}} + 1\right]} \frac{c}{a(t)r_a} \quad (\text{we})$$

$$\text{because of } \frac{1}{\beta(t)} = 2\sqrt{\frac{a(t)r_a}{R_s}} \quad \text{with} \quad \frac{c}{r_a} = \text{const} \quad \frac{r_a}{R_s} = \text{const} \quad R_s = \text{const} \quad (13a)$$

and

$$H_{a,lit}(t) = \frac{\dot{a}(t)r_a}{a(t)r_a} \quad (\text{literatur}) \quad .$$

The index a generally indicates the proximity to the observer ($r = r_a$).

In our theory, the numerator contains the constant physical speed of light c in a vacuum, while the current, i.e. variable, spatial expansion speed (da/dt) can be found at this point in the literature.

In the more recent past - time t_x - our distance from the coordinate origin $R_{xa} < R_{0a}$ was slightly smaller than the current one and the Hubble parameter was therefore correspondingly larger (also via the parameter β_x).

In the case of the Hubble parameter in literature, the - actually non-physical - spatial expansion speed da/dt can have been arbitrarily large and, in addition, the scale parameter $a(t)$ arbitrarily small. Both types of Hubble parameters therefore show completely different behavior!

In addition, our Hubble parameter is actually made up of physical quantities, while the Hubble parameter in the literature is only defined using the non-physical scale parameter $a(t)$, even if the latter can be assigned a suitable unit of measurement - e.g. Mpc. This means that $a(t)$ per se is not a physical distance. This meaning only applies to the real physical distance $R(t) = a(t)r$ and the differences that can be calculated from it.

The Hubble parameter is the proportionality factor between the Hubble speed $V = cz$ and a distance, i.e. the actual Hubble law applies

$$V = cz = H_{0a}D \approx \frac{1}{\left(\frac{1}{2\beta_0} + 1\right)} \frac{c}{R_{0a}} D \quad (\text{we}) \quad (14)$$

and

$$V_{lit} = cz = H_{0,lit}D_{lit} = \frac{\dot{a}_0}{a_0} D_{lit} = \frac{\dot{R}_{0a}}{R_{0a}} D_{lit} \quad (\text{literatur}) \quad .$$

For the redshift z it simply follows

$$z = \frac{H_{0a}}{c} D \approx \frac{1}{\left(\frac{1}{2\beta_0} + 1\right)} \frac{D}{R_{0a}} \quad (\text{we}) \quad (15)$$

and

$$z = \frac{H_{0,lit}}{c} D_{lit} = \frac{\dot{a}_0}{c} \frac{D_{lit}}{a_0} = \frac{\dot{R}_{0a}}{c} \frac{D_{lit}}{R_{0a}} \quad (\text{literatur}) \quad .$$

In the literature, the redshift z is therefore dependent on the ratio of the current speed of the observer (his galaxy) related to the origin of the coordinates to the speed of light in the product with the ratio of an object distance D_{lit} and the current distance of the observer's galaxy from the origin of the coordinates.

Our redshift, on the other hand, is dependent on the ratio of the light path distance D and the current distance of the observer galaxy from the coordinate origin R_{0a} and is besides proportional to the factor that contains the parameter β_0 .
Using the parameter β_0

$$\frac{1}{\beta_0} = 2 \sqrt{\frac{R_{0a}}{R_S}} \quad \text{with} \quad R_S = \frac{2MG}{c^2} \quad (16)$$

we see in our case

$$z = \frac{H_{0a}}{c} D \approx \frac{1}{\left(\sqrt{\frac{R_{0a}}{R_S}} + 1 \right)} \frac{D}{R_{0a}} \quad (\text{we}) \quad , \quad (17)$$

i.e. an direct dependence on the Schwarzschild radius R_S , or more precisely on the ratio R_{0a} to R_S .

Overall, it is somewhat unclear in the literature what exactly corresponds to the distance D_{lit} .

Figure 16 shows the difference between the non-approximated redshift distance D and the linear Hubble redshift distance that is approximated.

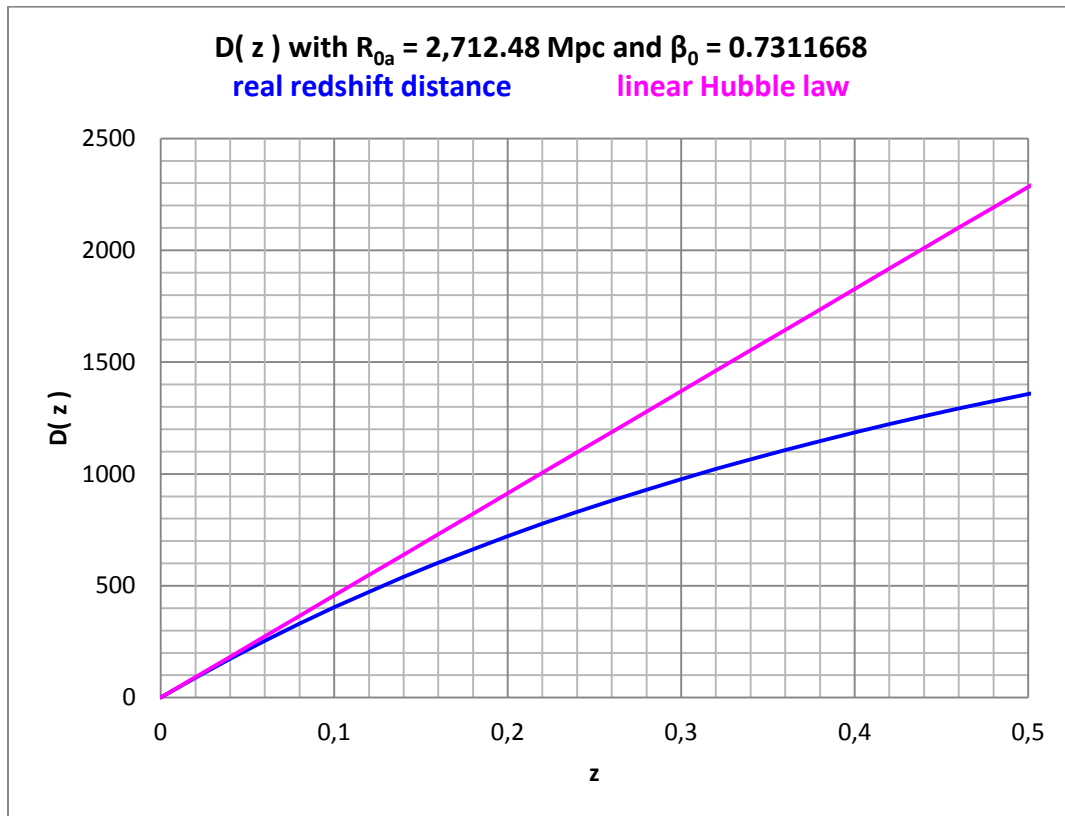


Figure 16. Non-approximated redshift distance D compared to the linear Hubble redshift distance.

It can be seen that the two curves already clearly separate from each other at $z \approx 0.04$, and that Hubble's law results in distances that are significantly too large for larger redshifts, so that it is no longer applicable from around this value.

Recall:

Of course, it should be noted that the Hubble parameter H_{0a} in our theory results from an approximation for small redshifts z .

4.2 Mean values

If we replace in the equation (I, 38)

$$m(z; m_{0a}, \beta_0) = 5 \log_{10} \left[\frac{1}{\beta_0} \left(1 - \frac{1}{\sqrt{1+z}} \right) + z \right] - 5 \log_{10}(1+z) + m_{0a} \quad (\text{I, 38})$$

the parameter m_{0a} using equation (I, 47)

$$m_{0a} = 5 \log_{10}(R_{0a}) - 5 + M \quad [R_{0a}] = pc \quad (\text{I,47})$$

we get

$$m(z; R_{0a}, \beta_0) = 5 \log_{10} \left[\frac{1}{\beta_0} \left(1 - \frac{1}{\sqrt{1+z}} \right) + z \right] - 5 \log_{10}(1+z) + 5 \log_{10}(R_{0a}) - 5 + M \quad . \quad (\text{18})$$

From this equation it follows immediately

$$R_{0a}(z, m; M, \beta_0) = \frac{(1+z)}{\left[\frac{1}{\beta_0} \left(1 - \frac{1}{\sqrt{1+z}} \right) + z \right]} 10^{\left[\frac{(m-M)}{5} + 1 \right]}, \quad (\text{19})$$

or, if we introduce the distance module $\mu = m - M$

$$R_{0a}(z; \mu, \beta_0) = \frac{(1+z)}{\left[\frac{1}{\beta_0} \left(1 - \frac{1}{\sqrt{1+z}} \right) + z \right]} 10^{\left(\frac{\mu}{5} + 1 \right)} \quad \text{mit} \quad \mu = m - M \quad . \quad (\text{20})$$

Note:

While the redshift z and the apparent magnitude m are actual measured variables, the distance module μ is to be regarded as a parameter because the absolute magnitude M cannot be measured directly.

The parameter β_0 is known to us from the evaluation of the Quasar catalog by Véron-Cetty [2]. In [4] the following parameters characterizing all 27 SNIa are given: absolute magnitude M_B , redshift z and maximum apparent magnitude m_B .

This allows us to calculate the associated $R_{0a, i}$ for all SNIa_{*i*} (*i* numbers the individual SNIa). Table 6 shows the result:

z_i	$R_{0a,i}$ [Mpc]	z_i	$R_{0a,i}$ [Mpc]	z_i	$R_{0a,i}$ [Mpc]
0.00435635	2,685.59	0.00229826	2,989.52	0.00845251	2,160.13
0.00350242	2,620.06	0.00349242	3,130.03	0.00456316	2,811.99
0.00435635	2,685.59	0.00621763	3,059.04	0.00151772	2,602.36
0.00229826	2,868.15	0.00807892	2,850.38	0.00435635	2,636.57
0.00350242	3,608.37	0.00748518	2,242.44	0.00350242	2,749.87
0.00350242	2,699.68	0.00435635	2,685.59	0.00434300	2,543.10
0.00517691	3,137.28	0.00661458	2,079.37	0.00482667	2,956.51
0.00629102	2,821.83	0.00435635	2,636.57	0.00470325	2,488.62

0.00456316	3,069.12	0.00567726	2,088.18	0.00423960	2,902.49
$\langle R_{0a} \rangle =$	2,733.65				

Table 6. Various distances $R_{0a,i}$ of the 27 SNI_a calculated using the distance modules μ_i .

It may seem strange that we get a different value for $R_{0a,i}$ for each SNI_a, which is actually the current physical distance of the observer from the coordinate origin ($r = 0$). In particular, the $R_{0a,i}$ for almost equal redshifts z_i should match!

But if we form the mean value of the 27 calculated values $R_{0a,i}$, we find $\langle R_{0a} \rangle \approx 2,733.65$ Mpc. This value is very close to the value $R_{0a} \approx 2,712.48$ Mpc, which we found above.

Overall, we must obvious conclude that the part of cosmology we are considering is essentially a science of averages.

In principle, this could be seen clearly from the beginning, if we retrospectively look a little more closely about the evaluation we carried out, e.g. the Quasar catalog and the subsequent finding of R_{0a} .

Only the consideration of a large number of cosmic objects results in the correct values of astrophysically and cosmologically relevant quantities, respectively, which then are partly mean values only.

5. Concluding remarks

The light path $D(z)$ of the photons through the expanding universe corresponds to a dynamic distance and is therefore an apparent one. This distance is not identical to the today's distance $D_0(z)$ between the objects. For every conceivable observer, the cosmic objects are not spatially where they appear at first glance! In cosmology nothing is what it seems to be if we look at distances.

Of course, all cosmologically relevant astrophysical objects have a today's distance D_0 . However, this is not observable, but we can calculate it.

Photons that are emitted at this distance from the observed galaxy cannot have reached us so far.

A fundamental property of quantum mechanics is that it can only make probability statements about the microscopic objects it deals with. Here it is seen that both the measuring and the theorizing astrophysics and cosmology, respectively, strictly speaking, can only make statements about mean values of very distant and large objects.

This may be one of the reasons why both theories - the theory for the extremely small and the theory for the extremely large - do not fit together; i.e. cannot be brought together.

Note of thanks:

I would like to thank my wife for the long-standing toleration and the corresponding endurance of my almost constant virtual absence. What would I be without her?!

6. Appendix

In this table appendix, we provide the essential data that we have used and some of the data that we have edited or generated for general purposes.

$\langle V \rangle_i$	$\langle z \rangle_i$	$\sigma_{m,i}$	$\langle V \rangle_i$	$\langle z \rangle_i$	$\sigma_{m,i}$	$\langle V \rangle_i$	$\langle z \rangle_i$	$\sigma_{m,i}$
17.12072194	0.269543711	1.25551062	19.5118161	1.28508799	0.79265674	19.7439932	1.86740102	0.8223715
18.42994924	0.434725324	0.69496662	19.4960406	1.30997857	0.82617985	19.7431839	1.90379949	0.8745066
18.77986464	0.514410603	0.68208433	19.5406994	1.33635871	0.79628275	19.73815	1.91629442	0.85608298
18.92177101	0.571495206	0.70268585	19.5648675	1.36044896	0.84936023	19.7370051	1.94113536	0.83013271
19.01993232	0.621120135	0.69571033	19.5526283	1.38646193	0.85285126	19.6390299	1.96661139	0.91303871

19.07454597	0.665043993	0.72385254	19.5667343	1.41249746	0.82510058	19.7247377	1.99498872	0.83486627
19.10685279	0.710045685	0.76943643	19.5917766	1.43823632	0.84883691	19.7073435	2.02761873	0.85770271
19.20756345	0.750830795	0.74776464	19.5835759	1.46348111	0.81435344	19.7225437	2.05895826	0.83582282
19.23878173	0.788362662	0.82397969	19.6146701	1.4877084	0.77561435	19.7209927	2.09067964	0.87548608
19.34673999	0.823077834	0.84208852	19.6560914	1.50872984	0.80798031	19.7166723	2.12286464	0.87190043
19.35605189	0.857111675	0.83026192	19.6421545	1.53039989	0.82193001	19.7562211	2.15726452	0.83914146
19.35379019	0.889902425	0.83562264	19.6730062	1.55031021	0.78502817	19.6955838	2.1915251	0.87311109
19.35354202	0.925268472	0.83309066	19.669718	1.57141117	0.81671189	19.7102256	2.23148844	0.89180926
19.36111675	0.958962211	0.80795962	19.691489	1.59370615	0.79783244	19.6203328	2.27565595	0.8814518
19.36687535	0.99085674	0.81407063	19.6689622	1.61663057	0.79869119	19.6516638	2.32895262	0.90747466
19.39208122	1.021072758	0.83447413	19.7130344	1.64024196	0.79496734	19.7034969	2.39616356	0.89952989
19.41216018	1.049862944	0.81581048	19.7208742	1.66227637	0.79948606	19.6915454	2.47184715	0.93743249
19.43737733	1.076128596	0.81828949	19.7568415	1.68460462	0.79535961	19.7660462	2.57089058	0.97654953
19.47736041	1.10186802	0.79353868	19.6973942	1.70912747	0.83259167	19.7708009	2.71401918	0.95905229
19.4307727	1.129618161	0.80360659	19.7453187	1.7323057	0.83488167	19.7781162	2.90122279	0.85728912
19.45345178	1.157690919	0.80262312	19.7723632	1.75403384	0.80160723	19.9208291	3.05796277	0.78948482
19.4499718	1.18469656	0.81310891	19.7568754	1.77625888	0.80788436	20.0279357	3.20401523	0.77347127
19.50609701	1.208890017	0.7810332	19.7599436	1.79742358	0.80969081	20.2283362	3.40521263	0.78550396
19.48940778	1.233098139	0.80906834	19.7587704	1.82113988	0.83363286	20.5549521	3.7254264	0.73269653
19.47597857	1.259028765	0.79685819	19.7435195	1.84394303	0.82211045	21.3169261	4.34427862	1.27303027

Table 7. Mean values from the Quasar data set used according to [2].

$\langle z \rangle_i$ (with $i = 1 \dots 75$) are the 75 mean values of the redshifts of the quasars in the redshift intervals formed.
 $\langle V \rangle_i$ are the associated 75 mean values of the apparent visual magnitude of the quasars.
 $\sigma_{m,i}$ are the standard deviations with respect to the apparent magnitudes (m-axis in the redshift-magnitude diagram).

z_i (end of interval)	N_i	z_i (end of interval)	N_i
0.24669	622	3.45369	128,884
0.49338	3,891	3.70038	130,205
0.74008	12,827	3.94708	131,357
0.98677	25,495	4.19377	132,019
1.23346	41,724	4.44046	132,432
1.48015	58,818	4.68715	132,669
1.72685	78,456	4.93385	132,848
1.97354	97,109	5.18054	132,902
2.22023	110,358	5.42723	132,924
2.46692	117,810	5.67392	132,932
2.71362	121,463	5.92062	132,949
2.96031	123,820	6.16731	132,972
3.20700	126,835	6.41400	132,977

Table 8. Numbers N_i summed up in the redshift intervals z_i of the quasars according to [2].

SNiA	μ_{TRGB}	μ_{Ceph}	μ or $\langle \mu \rangle$	m_{CSP_B0}	m_{SC_B}	m_B or $\langle m_B \rangle$	M_i or $\langle M_i \rangle$	V_{NED}	z
1980N	31.46		31.46	12.08		12.08	-19.38	1,306.00	0.004356347
1981B	30.96	30.91	30.94	11.64	11.62	11.63	-19.31	1,050.00	0.003502423
1981D	31.46		31.46	11.99		11.99	-19.47	1,306.00	0.004356347
1989B	30.22		30.22	11.16		11.16	-19.06	689.00	0.002298257
1990N		31.53	31.53	12.62	12.42	12.52	-19.01	1,050.00	0.003502423
1994D	31.00		31.00	11.76		11.76	-19.24	1,050.00	0.003502423

1994ae	32.27	32.07	32.17	12.94	12.92	12.93	-19.24	1,552.00	0.005176915
1995al	32.22	32.50	32.36	13.02	12.97	13.00	-19.37	1,886.00	0.006291019
1998aq		31.74	31.74	12.46	12.24	12.35	-19.39	1,368.00	0.004563157
1998bu	30.31		30.31	11.01		11.01	-19.30	689.00	0.002298257
2001el	31.32	31.31	31.32	12.30	12.20	12.25	-19.07	1,047.00	0.003492416
2002fk	32.50	32.52	32.51	13.33	13.20	13.27	-19.25	1,864.00	0.006217635
2003du		32.92	32.92	13.47	13.47	13.47	-19.45	2,422.00	0.008078922
2005cf		32.26	32.26	12.96	13.01	12.99	-19.28	2,244.00	0.007485178
2006dd	31.46		31.46	12.38		12.38	-19.08	1,306.00	0.004356347
2007af	31.82	31.79	31.81	12.72	12.70	12.71	-19.10	1,983.00	0.006614576
2007on	31.42		31.42	12.39		12.39	-19.03	1,306.00	0.004356347
2007sr	31.68	31.29	31.49	12.30	12.24	12.27	-19.22	1,702.00	0.005677261
2009ig		32.50	32.50	13.29	13.46	13.38	-19.13	2,534.00	0.008452514
2011by		31.59	31.59	12.63	12.49	12.56	-19.03	1,368.00	0.004563157
2011fe	29.08	29.14	29.11	9.82	9.75	9.79	-19.33	455.00	0.001517717
2011iv	31.42		31.42	12.03		12.03	-19.39	1,306.00	0.004356347
2012cg	31.00	31.08	31.04	11.72	11.55	11.64	-19.41	1,050.00	0.003502423
2012fr	31.36	31.31	31.34	12.09	11.92	12.01	-19.33	1,302.00	0.004343005
2012ht		31.91	31.91	12.66	12.70	12.68	-19.23	1,447.00	0.004826672
2013dy		31.50	31.50	12.23	12.31	12.27	-19.23	1,410.00	0.004703254
2015F		31.51	31.51	12.40	12.28	12.34	-19.17	1,271.00	0.0042396
						<M>=	-19.24		

Table 9. Summary of the data which we used from the 27 SNIa according to [4].

SNIa values that can be traced back to a mean value are marked in green (**bold**). The individual meanings of the data can be found in the article mentioned.

The data for the angular-size redshift diagram can be found in full in [3].

References

- [1] St. Haase, New derivation of redshift distance without using power expansions, viXra.org:2110.0024
- [2] M.-P. Véron-Cetty and P. Véron, A Catalogue of Quasars and Active Nuclei, 13th edition, March 2010, http://www.obs-hp.fr/catalogues/veron2_13/veron2_13.html
- [3] K. Nilsson, M. J. Valtonen, J. Kotilainen and T. Jaakkola, *Astro. J.* 413 (1993), 453.
- [4] W. L. Freedman u. a., The Carnegie-Chicago Hubble Program. VIII. An Independent Determination of the Hubble Constant Based on the Tip of the Red Giant Branch, arXiv.org:1907.05922
- [5] The Planck Collaboration: Planck 2018 results. VI. Cosmological parameters, arXiv:1807.06209
- [6] The Event Horizon Telescope Collaboration, *The Astrophysical Journal Letters*, 875:L1 (17pp), 2019 April 10, <https://doi.org/10.3847/2041-8213/ab0ec7>
- [7] de.wikipedia.org/wiki/Messier_87, abgerufen am 18.12.2021
- [8] de.wikipedia.org/wiki/Quasar, abgerufen am 18.12.2021
- [9] de.wikipedia.org/wiki/UDFj-39546284, abgerufen am 18.12.2021
- [10] G. Dautcourt, Was sind Quasare?, S. 68, Abb. 18, BSB B.G. Teubner Verlagsgesellschaft, 4. Auflage 1987

Copyright:

This text is subject to German and international copyright law, i.e. the publication, translation, transfer to other media, etc. - including parts - is permitted only with the prior permission of the author.

Copyright by Steffen Haase, Germany, Leipzig, 2022